frontiers | Frontiers in Oncology

TYPE Original Research
PUBLISHED 14 February 2024
DOI 10.3389/fonc.2024.1339126

OPEN ACCESS

EDITED BY
Xiangpan Li,
Renmin Hospital of Wuhan University, China

REVIEWED BY
Fuli Zhang,
People's Liberation Army General Hospital, China
Ma Yangguang,
The First Affiliated Hospital of Zhengzhou University, China
Bo Jiang,
Tianjin Medical University Cancer Institute and Hospital, China

*CORRESPONDENCE
Zhiqiang Liu
zhiqiang.liu@cicams.ac.cn
Hui Yan
hui.yan@cicams.ac.cn

†These authors have contributed equally to this work

RECEIVED 15 November 2023
ACCEPTED 26 January 2024
PUBLISHED 14 February 2024

CITATION
Huang P, Shang J, Hu Z, Liu Z and Yan H (2024) Predicting voxel-level dose distributions of single-isocenter volumetric modulated arc therapy treatment plan for multiple brain metastases.
Front. Oncol. 14:1339126.
doi: 10.3389/fonc.2024.1339126

Predicting voxel-level dose distributions of single-isocenter volumetric modulated arc therapy treatment plan for multiple brain metastases

Peng Huang†, Jiawen Shang†, Zhihui Hu, Zhiqiang Liu* and Hui Yan*

Department of Radiation Oncology, National Cancer Center/National Clinical Research Center for Cancer/Cancer Hospital, Chinese Academy of Medical Sciences and Peking Union Medical College, Beijing, China

Purpose: Brain metastasis is a common, life-threatening neurological problem for patients with cancer. Single-isocenter volumetric modulated arc therapy (VMAT) has been popularly used due to its highly conformal dose and short treatment time. Accurate prediction of its dose distribution can provide a general standard for evaluating the quality of treatment plan. In this study, a deep learning model is applied to the dose prediction of a single-isocenter VMAT treatment plan for radiotherapy of multiple brain metastases.

Method: A U-net with residual networks (U-ResNet) is employed for the task of dose prediction. The deep learning model is first trained from a database consisting of hundreds of historical treatment plans. The 3D dose distribution is then predicted with the input of the CT image and contours of regions of interest (ROIs). A total of 150 single-isocenter VMAT plans for multiple brain metastases are used for training and testing. The model performance is evaluated based on mean absolute error (MAE) and mean absolute differences of multiple dosimetric indexes (DIs), including (D_{max} and D_{mean}) for OARs, (D_{98}, D_{95}, D_{50}, and D_2) for PTVs, homogeneity index, and conformity index. The similarity between the predicted and clinically approved plan dose distribution is also evaluated.

Result: For 20 tested patients, the largest and smallest MAEs are 3.3% $\pm$ 3.6% and 1.3% $\pm$ 1.5%, respectively. The mean MAE for the 20 tested patients is 2.2% $\pm$ 0.7%. The mean absolute differences of D_{98}, D_{95}, D_{50}, and D_2 for PTV60, PTV52, PTV50, and PTV40 are less than 2.5%, 3.0%, 2.0%, and 3.0%, respectively. The prediction accuracy of OARs for D_{max} and D_{mean} is within 3.2% and 1.2%, respectively. The average DSC ranges from 0.86 to 1 for all tested patients.

Conclusion: U-ResNet is viable to produce accurate dose distribution that is comparable to those of the clinically approved treatment plans. The predicted results can be used to improve current treatment planning design, plan quality, efficiency, etc.

KEYWORDS

multiple brain metastases, volumetric modulated arc therapy, radiotherapy, deep learning, dose prediction

1 Introduction

Brain metastasis is the cancer that occurs when cancer cells from their original sites spread to the brain. The typical tumor sites causing brain metastasis are the lung, breast, colon, and kidney. Brain metastases could be single or multiple tumor sites in the brain (1, 2). The brain metastases could cause pressure on the brain. Also, the function of the surrounding brain tissue could be changed by the tumor. The symptoms of brain metastases include memory loss, seizures, headaches, etc. (3). The traditional treatment methods for brain metastases are surgery, whole-brain radiotherapy (WBRT), three-dimensional conformal radiation therapy (3D-CRT), hypo-fractionated stereotactic radiotherapy (SRT), and single-fraction stereotactic radiosurgery (SRS) (4–7).

WBRT and 3D-CRT have been traditionally used for the treatment of multiple brain metastases. However, WBRT can cause cognitive dysfunction or dementia, while 3D-CRT takes a long time to treat multiple brain metastases (8–10). In SRS/SRT, a higher accuracy of patient positioning is required. Recently, the developments of image-guided radiotherapy (IGRT) and volumetric modulated arc therapy (VMAT) techniques have provided precise target localization and quick dose delivery for patients under radiotherapy. The introduction of VMAT not only takes a short time in treatment delivery but also shows a highly conformal dose comparable to conventional SRS/SRT (11, 12). The treatment of brain metastases using VMAT has been accepted as a routine treatment modality in recent years (13, 14).

Compared to multiple-isocenter VMAT, single-isocenter VMAT is popular due to its quick and accurate beam delivery for the treatment of multiple brain metastases (15–17). However, to achieve an ideal dose distribution, a set of suitable plan optimization parameters (dose constraints and their weighting factors) is needed prior to the optimization of the treatment plan. Also, planners have to adjust these parameters manually during plan optimization, which usually takes several hours. To address this issue, knowledge-based planning (KBP) was proposed (18, 19) in the last decade. They implemented plan automation through optimization algorithms or templates from previously treated patients. These methods can partially reduce the effort involved in parameter fine-tuning but still require human involvement (20). Recently, the research interest in KBP has transitioned from classic machine learning methods to modern deep learning methods (21–25). Unlike classic machine learning methods, modern deep learning methods can directly learn features from the original data and predict 3D doses with high precision.

The recent development of the dose prediction model is mostly based on the U-Net structure, which consists of an encoder and decoder with skip connections. 2D U-Net was first applied to prostate IMRT plans by Nguyen et al. (21). After that, many efforts were made. Residual learning was introduced to the dose prediction model by several researchers (22–25), while dense connectivity was used to enhance feature representation capability by other researchers in their models (26–28). In addition, other types of networks, such as Resnet (27, 29, 30) and GAN (31–33), are also used for dose prediction. So far, the deep U-net-like architecture and its variants with various types of residual or dense blocks become the mainstream structure for dose prediction (34–38).

With the successful applications of deep learning models in predicting dose distribution for many primary tumor sites such as the lung (25, 26), head-and-neck (23, 28, 33, 34), and prostate (21, 35), it is interesting to investigate this application for brain metastasis. In the study, a deep U-net architecture (30), previously successfully applied to predict dose distribution for head-and-neck cancer patients, is used as the base model in predicting the dose distribution of the VMAT plan for brain metastasis. The rest of this paper is organized as follows: In Methods, the patient data, prediction model, and experimental settings are introduced in detail. In Results, the prediction accuracy of the deep learning model is evaluated by comparing it with the dose distribution of the clinically approved plans. Finally, the advantages and disadvantages of the prediction model are discussed, and future work is prospected in the Discussions.

2 Methods

2.1 Patient data

The dataset consists of 150 single-isocenter VMAT treatment plans designed for multiple brain metastases patients treated in our

institute during 2019–2022. All patient plans are made by medical physicists and approved by radiation oncologists for clinical treatment. The number of tumors in each patient is varied from one to four. PTVs include PTV60 for 31 patients, PTV52 for 41 patients, PTV50 for 34 patients, and PTV40 for 44 patients. Primary OARs include body, brain stem, spinal cord, left lens, right lens, left optic nerve, right optic nerve, and optic chiasm.

The 150 patient plans are randomly divided into three sets: 100 for training sets, 30 for validation sets, and 20 for testing sets. These VMAT plans are designed with two arcs and delivered with 6 MV beam energy. The input images are all rescaled to 256 × 256 × 21 matrixes (7 for CT images, 7 for contour image, and 7 channels for target prescriptions), and the output image is 256 × 256 × 1 matrixes (dose distributions on each slice). This study was conducted in accordance with the Declaration of Helsinki (as revised in 2013). This study was approved by the ethics committee of the National Cancer Center/Cancer Hospital, Chinese Academy of Medical Sciences, and Peking Union Medical College. The committee waived the written informed consent because this is a retrospective study.

2.2 Prediction model

The U-net with residual network (U-ResNet) model incorporating residual convolutional and de-convolutional blocks is shown in Figure 1. It consists of contracting and expansive paths. The contracting path follows convolutional layers and stacked building blocks of Identity-Block and Conv-Block to extract multiscale patient-specific features, doubling the number of feature maps at each step. The expansive path at each step consists of a de-convolutional block that halves the number of feature maps and concatenation with the corresponding feature map from the contracting path. The network ends with one de-convolution with 1 × 1 filters replacing 3 × 3 filters.

In the training and validation process, the training samples are augmented by randomly flipping, rotating, scaling, or shifting. The model is trained from scratch with the layer kernel weights initialized using Xavier uniform initialization. Adam optimizer (39) with a batch size of 4 is used for optimization. The initial learning rate (LR) is 1e −4, and the LR is reduced to 20% of its original value if the validation loss does not improve after 10 epochs. The training process is also stopped if the validation loss does not improve after 20 epochs. The model with the best performance on the validation samples is obtained for testing. The proposed network is implemented in Keras with TensorFlow as the backend on a workstation equipped with two NVIDIA GeForce 2080 Ti GPUs. The training process for a single model takes around 20 h. The prediction process for one case takes less than 1 s.

2.3 Model evaluation

The mean absolute error (MAE) is used to evaluate the accuracy of the predicted 3D dose distribution. It is the average error over all voxels of the body and is defined as Equation 1:

$$\mathrm{MAE}_k = \frac{1}{N_k}\sum_{i=1}^{N_k}|D_P - D_T| \times 100\,\% \tag{1}$$

Where N_k is the number of total voxels belonging to the kth structure. D_P and D_T are the predicted and ground-truth (or calculated) doses of the ith voxel. The voxel doses were normalized by the value of the prescription dose. Several traditional dosimetry indexes (DIs) ($D_{\max}$, D_{mean} for OARs and D_{98}, D_{95}, D_{50}, and D_2 for PTVs), conformity index (CI), and homogeneity index (HI) are also evaluated.

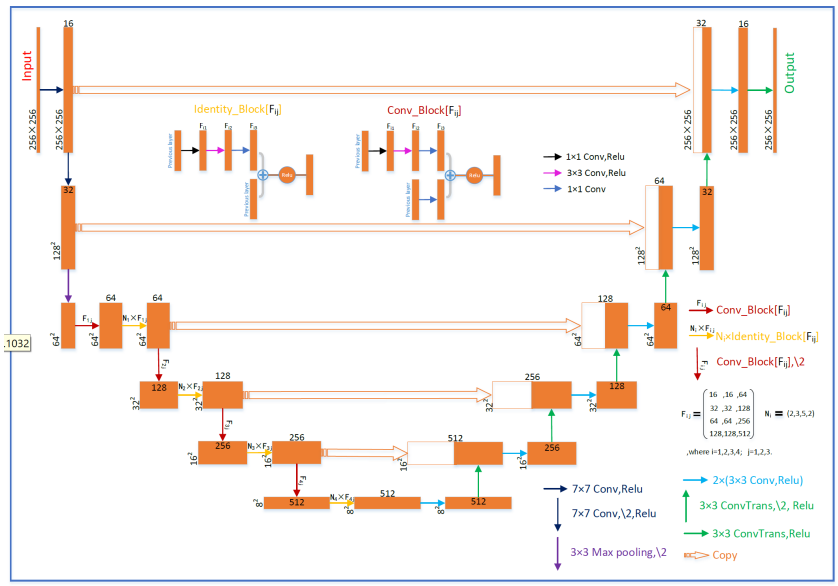

FIGURE 1
Schematic diagram of the deep U-net architecture.

CI formula is defined as Equation 2:

$$\mathrm{CI} = \frac{V_{T,\mathrm{ref}}}{V_T} \times \frac{V_{T,\mathrm{ref}}}{V_{\mathrm{ref}}} \quad (2)$$

$V_{T,\mathrm{ref}}$ is the volume of the target volume at which the received dose is equal to or greater than the reference dose; V_T is the volume of the target volume; V_{ref} is the volume at which the received dose is equal to or greater than the reference dose. The closer the value of CI is to 1, the better the target is covered. HI formula is defined as Equation 3:

$$\mathrm{HI} = \frac{D_2 - D_{98}}{D_{50}} \quad (3)$$

where D_n represents the minimum radiation dose received by n% of the volume of the radiation area. The closer the value of HI to 0, the better the uniformity of the target dose. In addition, the absolute differences in DI between predicted and clinically approved plans are evaluated as follows: $|\delta \mathrm{DI}| = |\mathrm{DI}_{\mathrm{clinical}} - \mathrm{DI}_{\mathrm{Predicted}}|$.

The dice similarity coefficient (DSC) between dose distributions is also evaluated and defined as Equation 4:

$$\mathrm{DSC}(A, B) = \frac{2|A \cap B|}{|A| + |B|} \quad (4)$$

where A represents the clinical isodose volume and B denotes the predicted isodose volume.

3 Results

Dose difference

The MAE plot for all 20 tested patients is shown in Figure 2. The largest and smallest MAEs are 3.3% ± 3.6% and 1.3% ± 1.5% within the patient's body, respectively. The largest and smallest MAEs are 5.2% ± 4.0% and 2.1% ± 1.7% within the targets, respectively. The average MAE is 2.2% ± 0.7% (relative to the prescription of PTV) within the body, and the average MAE is 3.6% ± 1.0% within targets.

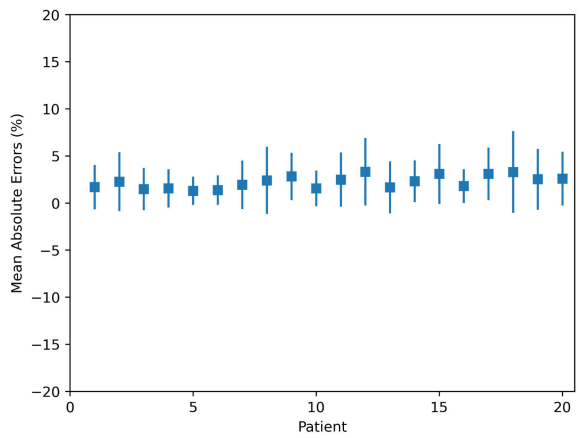

FIGURE 2
Mean absolute errors within the body for 20 tested patients.

Dosimetric index

For PTVs with multiple prescription doses, the dosimetric indexes are shown in Table 1. On average, the absolute differences of D_{98}, D_{95}, D_{50}, and D_2 for PTV60, PTV52, PTV50, and PTV40 are less than 2.5%, 3.0%, 2.0%, and 3.0%, respectively. There are no significant differences between predicted and clinically approved plan doses for PTVs. There are no significant differences from the predicted results for HI and CI. Regarding OARs, the dosimetric indexes of D_{max} and D_{mean} are shown in Table 2. The prediction accuracy for D_{max} and D_{mean} is between 3.2% and 1.2%. Six OARs for D_{max} and eight for D_{mean} were predicted within 2%. There is no significant difference between clinical and predicted results. For certain patients, the D_{max} and D_{mean} of OARs are close to 0, as they are far from PTV. This causes a large standard deviation of dosimetric results for these OARs. In general, the dosimetric indexes predicted by the model well match those from the clinically approved plans.

The examples of two patients' DVHs are presented in Figure 3. The clinical and predicted DVHs are shown in solid and dashed lines, respectively. Case 1 has two prescription doses (5,250 cGY and 6,000 cGy) and more OARs, while case 2 has one prescription dose (4,800 cGy) and three OARs. For OARs, the maximal dose discrepancy is presented in the higher dose region of the brain stem in both cases. For PTV, the maximal dose discrepancy is presented in the higher dose region of PTV5250 in case 1 and the lower dose region of PTV4800 in case 2.

Volumes similarity

The dice similarity coefficients between predicted and clinically approved plan doses for the different isodose volumes are calculated. As shown in Figure 4, the DSC versus isodose volumes for 20 tested patients are presented. The black curve denotes the averaged DSC curve, which usually ranges from 0 to 1, with 1 standing for ideal match. The averaged DSC for the different isodose volumes ranges from 0.86 to 1.

Corresponding to the cases shown in Figure 3, their clinical and predicted dose maps in 2D slices are presented in Figure 5. In the first and second columns, the clinical and predicted dose maps in axial view are displayed with a color wash pattern. The different images between the first and second columns are presented in the third column. For case 1, the predicted doses are higher than the clinical doses in two small regions on the left and right sides of PTV. For case 2, the predicted doses are less than the clinical doses on the left-bottom sides of PTV. Overall, the predicted and clinical doses are highly consistent.

4 Discussions

In this study, an advanced deep learning model is applied to predict 3D dose distribution based on our clinical dataset. As far as we know, there is no deep learning model used in predicting the dose of VMAT plans for multiple brain metastases. Using 150 brain

10.3389/fonc.2024.1339126

TABLE 1 Statistics of dosimetric indexes for PTVs of 20 tested patients.

PTVs	Dosimetric indexes	Clinically approved	Model predicted	|δDI|	*p*-value
PTV60	D_{98} (Gy)	60.1 ± 1.0	58.9 ± 1.5	2.1% ± 2.1%	0.054
	D_{95} (Gy)	60.7 ± 0.8	59.5 ± 1.2	2.2% ± 1.9%	0.063
	D_{50} (Gy)	62.8 ± 1.2	62.4 ± 1.0	1.9% ± 2.0%	0.541
	D_2 (Gy)	65.0 ± 2.3	64.9 ± 1.5	2.5% ± 1.4%	0.947
	HI	0.1 ± 0.0	0.1 ± 0.0	0.0% ± 0.0	0.336
	CI	1.0 ± 0.0	1.0 ± 0.0	0.0% ± 0.0	0.282
PTV52	D_{98} (Gy)	50.7 ± 0.7	49.4 ± 1.8	3.0% ± 1.2%	0.142
	D_{95} (Gy)	52.2 ± 0.1	51.3 ± 0.9	1.8% ± 1.5%	0.116
	D_{50} (Gy)	57.1 ± 0.8	56.1 ± 0.7	2.1% ± 1.4%	0.104
	D_2 (Gy)	60.5 ± 2.1	59.7 ± 1.6	2.0% ± 1.9%	0.271
	HI	0.2 ± 0.0	0.2 ± 0.0	0.0% ± 0.0	0.657
	CI	1.0 ± 0.0	0.9 ± 0.0	0.0% ± 0.0	0.087
PTV50	D_{98} (Gy)	49.0 ± 0.6	48.2 ± 0.4	1.4% ± 2.0%	0.489
	D_{95} (Gy)	50.3 ± 0.4	49.3 ± 0.3	2.0% ± 1.4%	0.295
	D_{50} (Gy)	55.5 ± 0.5	54.7 ± 0.2	1.5% ± 0.7%	0.208
	D_2 (Gy)	59.4 ± 0.8	59.4 ± 0.6	0.2% ± 0.2%	0.627
	HI	0.2 ± 0.0	0.2 ± 0.0	0.0% ± 0.0	0.391
	CI	1.0 ± 0.0	0.9 ± 0.0	0.0% ± 0.0	0.353
PTV40	D_{98} (Gy)	38.3 ± 0.6	37.9 ± 0.4	1.0% ± 1.2%	0.207
	D_{95} (Gy)	40.0 ± 0.1	39.4 ± 0.8	1.6% ± 1.6%	0.225
	D_{50} (Gy)	43.3 ± 1.1	43.6 ± 0.3	2.6% ± 1.6%	0.741
	D_2 (Gy)	45.9 ± 1.6	46.5 ± 0.4	3.0% ± 1.1%	0.400
	HI	0.2 ± 0.0	0.2 ± 0.0	0.0% ± 0.0	0.453
	CI	1.0 ± 0.0	0.9 ± 0.0	0.0% ± 0.0	0.350

TABLE 2 Statistics of dosimetric metrics for OARs in 20 tested patients.

	Dmax (Gy)				Dmean (Gy)			
OARs and body	Clinically approved	Model predicted	|δDI| (%)	*p*-value	Clinically approved	Model predicted	|δDI| (%)	*p*-value
Brain stem	4.7 ± 4.8	4.2 ± 4.9	2.8 ± 2.1	0.247	1.1 ± 1.1	1.1 ± 1.6	0.9 ± 1.0	0.990
Spinal cord	0.7 ± 1.7	0.7 ± 1.6	0.6 ± 1.3	0.961	0.1 ± 0.2	0.0 ± 0.1	0.1 ± 0.2	0.113
Center lens	0.6 ± 0.8	0.8 ± 1.0	0.7 ± 0.7	0.076	0.4 ± 0.7	0.6 ± 0.9	0.6 ± 0.5	0.219
Right lens	0.8 ± 0.9	0.7 ± 0.8	0.6 ± 0.6	0.450	0.5 ± 0.7	0.4 ± 0.5	0.6 ± 0.5	0.248
Center optic nerve	1.7 ± 3.0	1.4 ± 2.5	0.9 ± 0.9	0.161	1.1 ± 2.1	1.0 ± 1.9	0.7 ± 0.6	0.302
Right optic nerve	1.3 ± 1.5	1.1 ± 1.6	1.2 ± 1.1	0.233	0.7 ± 1.0	0.6 ± 1.1	0.8 ± 0.8	0.508
Optic chiasm	3.7 ± 4.5	3.8 ± 6.0	1.8 ± 3.2	0.857	1.3 ± 2.0	1.2 ± 2.0	1.2 ± 1.4	0.789
Body	60.2 ± 7.3	59.4 ± 7.5	3.2 ± 2.5	0.137	1.6 ± 1.1	1.6 ± 1.0	0.3 ± 0.2	0.705

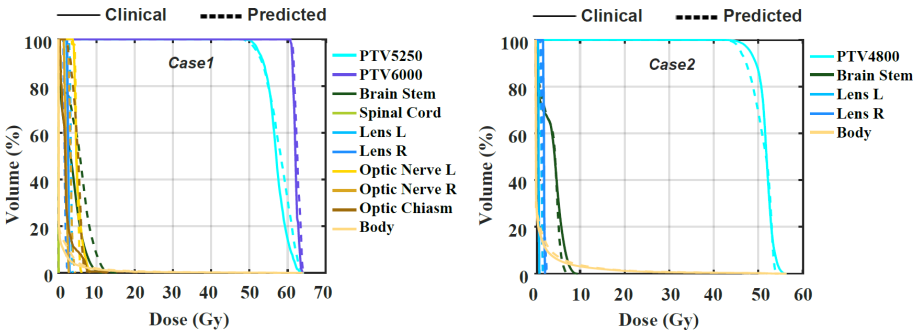

FIGURE 3
The comparison of the clinical and predicted DVHs for two cases.

metastases from VMAT plans, the U-ResNet model exhibits accurate dose distribution and high efficiency. As shown in Table 1, the mean prediction errors range from 1.9% to 2.5%, 1.8% to 3.0%, 0.2% to 2.0%, and 1.0% to 3.0% for PTV60, PTV52, PTV50, and PTV40, respectively. For the absolute value of the PTV dose, the mean value of the predicted plan doses is slightly less than that of the clinically approved plan doses. This may be due to the inclusion of various target prescriptions in a single model, where the varying combinations of prescriptions may impact the prediction accuracy of the target dose. The limited number of samples and larger variation of tumor sites may be another reason. There is no significant difference in dosimetric indexes between clinically approved and predicted plan doses. Although the results demonstrate that the prediction accuracy is acceptable for clinical use, there is still a certain room for improvement.

Although U-ResNet succeeded in dose prediction, as reported by many researchers, there is still a lot of room for improvement. The receptive field would be enlarged increasingly by the stacked multiple convolution layers in the decoder. However, the network's capability to catch features in multiscale resolution could be limited. The predicted voxel dose is affected not only by the neighboring voxels but also by the spatial distribution between PTVs and OARs. Thus, to extract multiscale features from the image simultaneously, the introduction of pyramid blocks is needed. We will test the model with the modules in a serial or parallel manner in the future, which could further improve the performance of the prediction model.

There are several challenges to this study. First, it is difficult to collect hundreds of VMAT plans with similar locations and shapes of tumor mass for model learning. In the case of multiple brain metastases, the number of tumor masses and their locations could vary considerably among patients. The limited number of samples and larger variation of tumor sites and shapes will make it hard to learn a solid pattern for a learning model. A more effective model or strategy is needed in dealing with such situations for multiple brain metastases. Second, the introduction of U-ResNet increases the

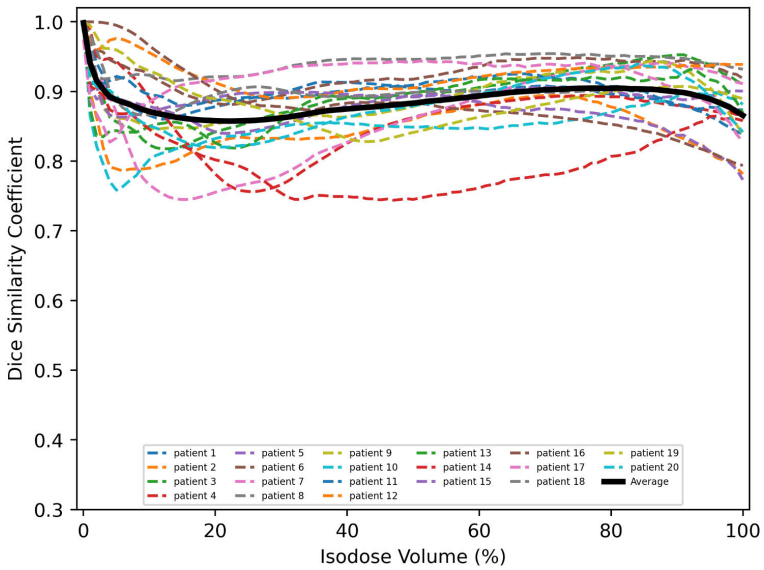

FIGURE 4
Similarity between clinical and predicted isodose distributions for 20 tested patients.

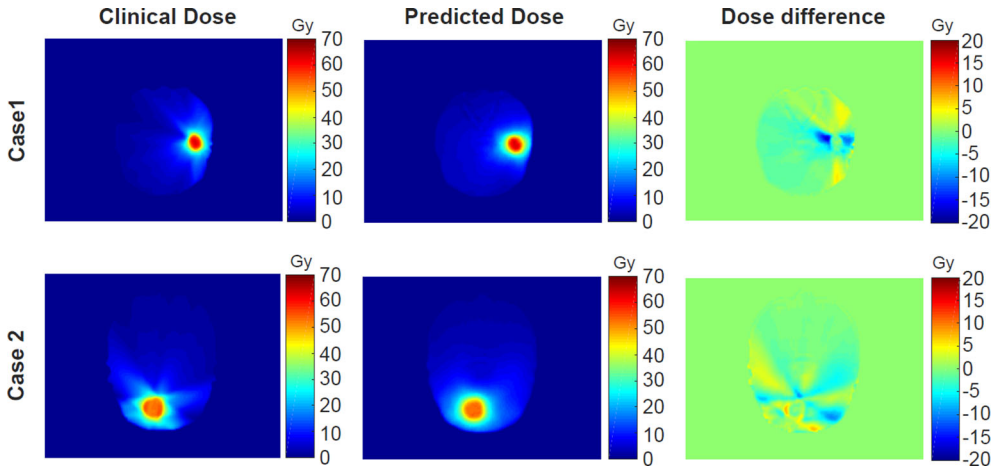

FIGURE 5
The comparison of the clinical and predicted dose maps for two cases.

complexity and time of model training. As tested, the time on model training is about 20 h on a workstation equipped with two NVIDIA GeForce 2080Ti GPUs. In the future, we plan to further fine-tune the basic 3D model and build a more memory-efficient mechanism for higher performance.

5 Conclusions

In this work, we evaluated a deep-learning model for 3D voxel-by-voxel dose prediction. It is capable of producing accurate dose distribution of VMAT plans for multiple brain metastases. As an improvement over the single U-Net or ResNet, it is a powerful model that can automatically correlate ROI voxel with dose voxel to achieve high-precise 3D dose prediction. The predicted results can be used to improve current treatment planning design, plan quality, and efficiency.

Data availability statement

The original contributions presented in the study are included in the article/supplementary material. Further inquiries can be directed to the corresponding authors.

Author contributions

PH: Conceptualization, Methodology, Writing – original draft. JS: Methodology, Software, Validation, Writing – original draft. ZH: Data curation, Formal Analysis, Validation, Writing – review & editing. ZL: Funding acquisition, Project administration, Resources, Writing – review & editing. HY: Conceptualization, Funding acquisition, Supervision, Writing – review & editing.

Funding

The author(s) declare financial support was received for the research, authorship, and/or publication of this article. This work is supported by the Special Research Fund for Central Universities, Peking Union Medical College, CAMS Innovation Fund for Medical Sciences (CIFMS) (2022-I2M-C&T-B-075), the Beijing Hope Run Special Fund of Cancer Foundation of China (LC2021B01), the Natural Science Foundation (NSF) of China (No. 11975312), and the Beijing Municipal Natural Science Foundation (7202170).

Conflict of interest

The authors declare that the research was conducted in the absence of any commercial or financial relationships that could be construed as a potential conflict of interest.

Publisher's note

References

1. Soffietti R, Ruda R, Mutani R. Management of brain metastases. *J Neurol*. (2002) 249:1357–69. doi: 10.1007/s00415-002-0870-6

2. Zimm S, Wampler GL, Stablein D, Hazra T, Young HF. Intracerebral metastases in solid-tumor patients: natural history and results of treatment. *Cancer*. (1981) 48:384–94. doi: 10.1002/1097-0142(19810715)48:2<384::AID-CNCR2820480227>3.0.CO;2-8

3. Posner JB. *Neurologic complications of cancer*. Philadelphia, PA: FA Davies (1995).

4. Soffietti R, Costanza A, Laguzzi E, Nobile M, Rudà R. Radiotherapy and chemotherapy of brain metastases. *J Neurooncol*. (2005) 75:31–42. doi: 10.1007/s11060-004-8096-3

5. Richards CM, Khuntia D, Mehta MP. Therapeutic management of metastatic brain tumors. *Crit Rev Oncol Hematol*. (2007) 61:70–8. doi: 10.1016/j.critrevonc.2006.06.012

6. Shibamoto Y, Sugie C, Iwata H. Radiotherapy for metastatic brain tumors. *Int J Clin Oncol*. (2009) 14:281–8. doi: 10.1007/s10147-009-0915-2

7. Caffo M, Barresi V, Caruso G, Cutugno M, la Fata G, Venza M, et al. Innovative therapeutic strategies in the treatment of brain metastases. *Int J Mol Sci*. (2013) 14:2135–74. doi: 10.3390/ijms14012135

8. Kocher M, Soffietti R, Abacioglu U, Villà S, Fauchon F, Baumert BG, et al. Adjuvant whole-brain radiotherapy versus observation after radiosurgery or surgical resection of one to three cerebral metastases: results of the EORTC 22952-26001 study. *J Clin Oncol*. (2011) 29:134–41. doi: 10.1200/JCO.2010.30.1655

9. Boehling NS, Chang EL, Ma LJ, Phan N, Yeung R, Sahga A. Stereotactic radiosurgery for brain metastases: current status and future directions. *J Radiat Oncol*. (2012) 1:245–53. doi: 10.1007/s13566-012-0043-x

10. Fowler JF, Welsh JS, Howard SP. Loss of biological effect in prolonged fraction delivery. *Int J Radiat Oncol Biol Phys*. (2004) 59:242–9. doi: 10.1016/j.ijrobp.2004.01.004

11. Wolff HA, Wagner DM, Christiansen H, Hess CF, Vorwerk H. Single fraction radiosurgery using Rapid Arc for treatment of intracranial targets. *Radiat Oncol*. (2010) 5:77. doi: 10.1186/1748-717X-5-77

12. Clark GM, Popple RA, Young PE, Fiveash JB. Feasibility of single-isocenter volumetric modulated arc radiosurgery for treatment of multiple brain metastases. *Int J Radiat Oncol Biol Phys*. (2010) 76:296–302. doi: 10.1016/j.ijrobp.2009.05.029

13. Mayo CS, Ding L, Addesa A, Kadish S, Fitzgerald TJ, Moser R. Initial experience with volumetric IMRT (RapidArc) for intracranial stereotactic radiosurgery. *Int J Radiat Oncol Biol Phys*. (2010) 75:253–9. doi: 10.1016/j.ijrobp.2009.10.005

14. Teoh M, Clark CH, Wood K, Whitaker S, Nisbet A. Volumetric modulated arc therapy: a re- view of current literature and clinical use in practice. *Br Inst Radiol*. (2011) 84:967–96. doi: 10.1259/bjr/22373346

15. Iwai Y, Ozawa S, Ageishi T, Pellegrini R, Yoda K. Feasibility of single-isocenter, multi-arc non-coplanar volumetric modulated arc therapy for multiple brain tumors using a linear accelerator with a 160-leaf multileaf collimator: a phantom study. *J Radiat Res*. (2014) 55:1015–20. doi: 10.1093/jrr/rru042

16. Kang J, Ford EC, Smith K, Wong J, McNutt TR. A method for optimizing LINAC treatment geometry for volumetric modulated arc therapy of multiple brain metastases. *Med Phys*. (2010) 37:4146–54. doi: 10.1118/1.3455286

17. Clark GM, Popple RA, Prendergast BM, Spencer SA, Thomas EM, Stewart JG, et al. Plan quality and treatment planning technique for single isocenter cranial radiosurgery with volumetric modulated arc therapy. *Pract Radiat Oncol*. (2012) 2:306–13. doi: 10.1016/j.prro.2011.12.003

18. Good D, Lo J, Lee WR, Wu QJ, Yin FF, Das SK. A knowledge-based approach to improving and homogenizing intensity modulated radiation therapy planning quality among treatment centers: an example application to prostate cancer planning. *Int J Radiat Oncol Biol Phys*. (2013) 87:176–81. doi: 10.1016/j.ijrobp.2013.03.015

19. Nwankwo O, Mekdash H, Sihono DS, Wenz F, Glatting G. Knowledge-based radiation therapy (KBRT) treatment planning versus planning by experts: validation of a KBRT algorithm for prostate cancer treatment planning. *Radiat Oncol*. (2015) 10:111. doi: 10.1186/s13014-015-0416-6

20. Shiraishi S, Moore KL. Knowledge-based prediction of three-dimensional dose distributions for external beam radiotherapy. *Med Phys*. (2016) 43:378. doi: 10.1118/1.4938583

21. Nguyen D, Long T, Jia X, Lu W, Gu X, Iqbal Z, et al. A feasibility study for predicting optimal radiation therapy dose distributions of prostate cancer patients from patient anatomy using deep learning. *Sci Rep*. (2019) 9:1076. doi: 10.1038/s41598-018-37741-x

22. Jiang D, Yan H, Chang N, Li T, Mao R, Du C, et al. Convolutional neural network-based dosimetry evaluation of esophageal radiation treatment planning. *Med Phys*. (2020) 47:4735–42. doi: 10.1002/mp.14434

23. Fan J, Wang J, Chen Z, Hu C, Zhang Z, Hu W. Automatic treatment planning based on three-dimensional dose distribution predicted from deep learning technique. *Med Phys*. (2019) 46:370–81. doi: 10.1002/mp.13271

24. Chen X, Men K, Li Y, Yi J, Dai J. A feasibility study on an automated method to generate patient-specific dose distributions for radiotherapy using deep learning. *Med Phys*. (2019) 46:56–64. doi: 10.1002/mp.13262

25. Kearney V, Chan JW, Haaf S, Descovich M, Solberg TD. DoseNet: a volumetric dose prediction algorithm using 3D fully-convolutional neural networks. *Phys Med Biol*. (2018) 63:235022. doi: 10.1088/1361-6560/aaef74

26. Barragán-Montero AM, Nguyen D, Lu W, Lin MH, Norouzi-Kandalan R, Geets X, et al. Three-dimensional dose prediction for lung IMRT patients with deep neural networks: robust learning from heterogeneous beam configurations. *Med Phys*. (2019) 46:3679–91. doi: 10.1002/mp.13597

27. Zhang J, Liu S, Yan H, Li T, Mao R, Liu J. Predicting voxel-level dose distributions for esophageal radiotherapy using densely connected network with dilated convolutions. *Phys Med Biol*. (2020) 65:205013. doi: 10.1088/1361-6560/aba87b

28. Nguyen D, Jia X, Sher D, Lin MH, Iqbal Z, Liu H, et al. 3D radiotherapy dose prediction on head and neck cancer patients with a hierarchically densely connected U-net deep learning architecture. *Phys Med Biol*. (2019) 64:065020. doi: 10.1088/1361-6560/ab039b

29. Yan H, Liu S, Zhang J, Liu J, Li T. Utilizing pre-determined beam orientation information in dose prediction by 3D fully-connected network for intensity modulated radiotherapy. *Quant Imaging Med Surg*. (2021) 11:4742–52. doi: 10.21037/qims-20-1076

30. Liu Z, Fan J, Li M, Yan H, Hu Z, Huang P, et al. A deep learning method for prediction of three-dimensional dose distribution of helical tomotherapy. *Med Phys*. (2019) 46:1972–83. doi: 10.1002/mp.13490

31. Babier A, Mahmood R, McNiven AL, Diamant A, Chan TCY. Knowledge-based automated planning with three-dimensional generative adversarial networks. *Med Phys*. (2020) 47:297–306. doi: 10.1002/mp.13896

32. Zhan B, Xiao J, Cao C, Peng X, Zu C, Zhou J, et al. Multi-constraint generative adversarial network for dose prediction in radiotherapy. *Med Image Anal*. (2022) 77:102339. doi: 10.1016/j.media.2021.102339

33. Gu X, Strijbis VIJ, Slotman BJ, Dahele MR, Verbakel WFAR. Dose distribution prediction for head-and-neck cancer radiotherapy using a generative adversarial network: influence of input data. *Front Oncol*. (2023) 13:1251132. doi: 10.3389/fonc.2023.1251132

34. Osman AFI, Tamam NM, Yousif YAM. A comparative study of deep learning-based knowledge-based planning methods for 3D dose distribution prediction of head and neck. *J Appl Clin Med Phys*. (2023) 24:e14015. doi: 10.1002/acm2.14015

35. Kadoya N, Kimura Y, Tozuka R, Tanaka S, Arai K, Katsuta Y, et al. Evaluation of deep learning-based deliverable VMAT plan generated by prototype software for automated planning for prostate cancer patients. *J Radiat Res*. (2023) 64:842–9. doi: 10.1093/jrr/rrad058

36. Gronberg MP, Gay SS, Netherton TJ, Rhee DJ, Court LE, Cardenas CE. Technical Note: Dose prediction for head and neck radiotherapy using a three-dimensional dense dilated U-net architecture. *Med Phys*. (2021) 48:5567–73. doi: 10.1002/mp.14827

37. Gronberg MP, Beadle BM, Garden AS, Skinner H, Gay S, Netherton T, et al. Deep learning-based dose prediction for automated, individualized quality assurance of head and neck radiation therapy plans. *Pract Radiat Oncol*. (2023) 13:e282–91. doi: 10.1016/j.prro.2022.12.003

38. Gronberg MP, Jhingran A, Netherton TJ, Gay SS, Cardenas CE, Chung C, et al. Deep learning-based dose prediction to improve the plan quality of volumetric modulated arc therapy for gynecologic cancers. *Med Phys*. (2023) 50:6639–48. doi: 10.1002/mp.16735

39. Kingma DP, Ba J. Adam: A method for stochastic optimization. *arXiv:1412.6980* (2014).